Crystal Structures and Magnetic Properties of a Novel Layer Perovskite System: (3-Picoliniumylammonium)CuX_4 (X = Cl, Br)

Greg S. Long, Mingyi Wei, and Roger D. Willett*

Department of Chemistry, Washington State University, Pullman, Washington 99164

Received July 18, 1996[⊗]

The compounds $(C_6N_2H_{10})CuX_4$, where the cation is diprotonated 3-picolylamine and X = Cl^- or Br^-, form an unusual variant of the normal antiferrodistortive A_2CuX_4 lattice [$(C_6N_2H_{10})CuCl_4$, orthorhombic, $Pna2_1$, a = 7.747(1), b = 24.960(2), and c = 17.041(1) Å, Z = 12; $(C_6N_2H_{10})CuBr_4$, orthorhombic, $Pna2_1$, a = 8.133(1), b = 26.129(1), and c = 17.148(1) Å, Z = 12]. The structures contain ribbons of the antiferrodistortive sheets which are six copper atoms wide. The central four Cu(II) ions have the usual elongated octahedral coordination, while on each edge are CuX_4^{2-} ions which have a distorted tetrahedral geometry. Long Cu···X interactions (4.000 and 4.124 Å for the Cl and Br salts, respectively) between these terminating anions link the ribbons together into sheets. The organic cations provide overall stability to the lattice and link adjacent sheets together, forcing the existence of short two-halide X···X contacts between sheets (average Cl···Cl = 4.629 Å, Br···Br = 4.425 Å). While the changes in the semicoordinate Cu···X distances upon replacement of Cl by Br mirror the change in ionic radius, the X···X distances actually decrease when the larger bromide ion is introduced. This is because these distances are largely dictated by the size of the organic cation. The magnetic data for both salts show the presence of predominant ferromagnetic interactions at high temperature. The Cl salt orders antiferromagnetically at T_c = 5.7 K, and the susceptibility data can be fit to a $S = {}^1/_2$ Heisenberg model for antiferromagnetically coupled ferromagnetic layers with a mean in-plane exchange constant of J/k = 8.13 K and an interlayer exchange constant of J'/k = 1.22 K. The corresponding values for the Br salt are T_c = 18.9 K, J/k = 21.3 K, and J'/k = 5.87 K The increase in magnitude of the exchange constants and ordering temperature of the Br salt relative to the Cl salt is consistent with the increase in ionic radius of Br^- relative to Cl^-.

Introduction

Recently there has been much interest in the properties of layer perovskite structures because of their support of high-temperature superconductivity.[1] The dominant structural characteristic of the Cu(II) oxide members of this class of compounds is the ferrodistortive nature of the Jahn−Teller distortion of the Cu(II) coordination sphere. This leads to linear symmetrical Cu−O−Cu linkages and strong antiferromagnetic exchange coupling. The magnetic properties of the corresponding halide analogs have long been of importance in low-dimensional magnetism.[2] These A_2CuX_4 compounds contain an antiferrodistortive version of the layer perovskite lattice. In these structures, the directions of the Jahn−Teller elongation lie approximately in the plane of the layer but with the adjacent elongation directions rotated by 90°. The result is that asymmetrical Cu−X···Cu linkages exist which lead to ferromagnetic exchange coupling within the layer since the magnetic orbitals on adjacent Cu(II) ions are orthogonal.

Two general classes of M(II) halide layer perovskite structures exist, the monoammonium series,[3] $(RNH_3)_2MX_4$, and the diammonium series,[4] $(NH_3RNH_3)MX_4$. In the former, the perovskite layer is sheathed by two layers of RNH_3^+ cations. Stacking of these sheathed layers leads to the formation of a crystalline bilayer structure. In the latter, the dications bridge between adjacent perovskite layers. In general, the R group in both classes is restricted to a straight chain aliphatic group or, possibly, a chain containing one phenyl group. This is a result of the restriction on the cross section of the R group imposed by the corner-shared octahedral structure for the layer. In addition, steric constraints imposed by corner-sharing of the MX_6 octahedra generally require that the organic cation be a monosubstituted ammonium ion. However, when M = Cu, additional flexibility in the choice of organic cation is attained because of the variable length of the Cu···X linkages. For example, the layer perovskite structure is observed with the formula $(ACl)_2CuCl_4$ when A is the bulky *N*-benzylpiperazinium dication.[3d] Now, however, the cation−layer interactions involve a disubstituted ammonium group that hydrogen bonds into the perovskite layer. In order to accommodate the bulky cation, one of the semicoordinate Cu···Cl bonds lengthens to over 3.9 Å. A second example is in the (3-ammoniopyridinium)CuX_4 salts.[5a] Here, the asymmetrical dication bridges between layers, with both the $-NH_3^+$ group and the pyridinium N−H group hydrogen bonding to the halide ions in the layer.

Several major magneto−structural correlations have arisen out of the studies on the Cu(II) halide layer perovskites. It has been observed that the ferromagnetic intralayer exchange (labeled J_{1h} since it involves a single halogen bridge) decreases monotonically as the Cu···X distance increases.[5] This is anticipated since the coulomb and exchange integrals will

[⊗] Abstract published in *Advance ACS Abstracts*, June 1, 1997.

(1) La Placa, S. J.; Bringley, J. F.; Scott, B. A. *Acta Crystallogr.* **1993**, *C49*, 1415.
(2) (a) De Jongh, L. J.; Miedema, A. R. *Adv. Phys.* **1974**, *23*, 1. (b) Richards, P. M.; Salamon, M. B. *Phys. Rev. B.* **1974**, *9*, 32. (c) Kite, T. M.; Drumheller, J. E. *J. Magn. Reson.* **1983**, *54*, 253.
(3) (a) Steadman, J. P.; Willett, R. D. *Inorg. Chim. Acta* **1970**, *4*, 367. (b) Barendregt, F.; Schenk, H. *Physica* **1970**, *49*, 465. (c) Willett, R. D. *Acta Crystallogr.* **1990**, *C46*, 565. (d) Antolini, L.; Menabue, L.; Marcotrigiano, G.; Pellacani, G. C. *Inorg. Chim. Acta* **1982**, *58*, 193.
(4) (a) Ferguson, G. L.; Zaslow, B. *Acta Crystallogr.* **1971**, *B27*, 849. (b) Garland, J. K.; Emerson, K.; Pressprich, M. *Acta Crystallogr.* **1990**, *C46*, 1603. (c) Halvorson, K.; Willett, R. D. *Acta Crystallogr.* **1988**, *C44*, 2071. (d) Tichy, K.; Benes, J.; Holg, W.; Arend, H. *Acta Crystallogr.* **1978**, *B34*, 2970.
(5) (a) Middleton, M.; Place, H.; Willett, R. D. *J. Am. Chem. Soc.* **1988**, *110*, 8639. (b) Landee, C. P.; Halvorson, K.; Willett, R. D. *J. Appl. Phys.* **1987**, *61*, 3295.

S0020-1669(96)00849-X CCC: $14.00

Table 1. Crystal Data and Experimental Details for (3-picoliniumylammonium)CuX_4

empirical formula	$(C_6N_2H_{10})CuCl_4$	$(C_6N_2H_{10})CuBr_4$
fw	315.5	493.3
cryst system	orthorhombic	orthorhombic
space group	*Pna*2_1 (No. 33)	*Pna*2_1 (No. 33)
a, Å	7.747(1)	8.133(1)
b, Å	24.960(2)	26.129(1)
c, Å	17.041(1)	17.148(1)
V, Å^3	3295.5(12)	3644.07(10)
Z	12	12
temp, °C	21	21
λ, Å	Mo Kα (0.710 73)	Cu Kα (1.541 82)
ρ_{calcd}, g cm^{-3}	1.846	2.698
μ(Mo Kα), cm^{-1}	29.13	176.38
R, %[a]	5.39	4.77
R_w, %[b]	6.84	6.33

[a] $R = \sum||F_o| - |F_c||/\sum|F_o|$. [b] $R_w = \sum w(|F_o| - |F_c|)^2/\sum|F_o|^2$.

decrease as this distance increases. In addition, it has been observed that J_{1h}(Br) is about 50% larger than J_{1h}(Cl), for an equal Cu···X distance.[6] Again, this is reasonable considering the effect that will be found by replacing the smaller chloride ion by the larger bromide ion.

In the dication $(NH_3RNH_3)MX_4$ series, an additional magnetic interaction is important for small R groups. In these structures, the perovskite layers assume an eclipsed structure and short X···X contacts exist between layers. The direct overlap of magnetic orbitals in this fashion leads to an antiferromagnetic coupling between layers (labeled J_{2h}, since the exchange pathway involves two halide ions). It has been observed experimentally[7] and confirmed theoretically[8] that J_{2h} increases dramatically as the X···X decreases. Indeed, for the bromide salt with R = C_2H_4, $|J_{2h}| > J_{1h}$, so that the system behaves as a pseudo-one-dimensional antiferromagnetic system rather than a pseudo-two-dimensional ferromagnetic system. Since the interlayer distance is largely dictated by the size of the dication and not the size of the halide ion, the magnitude of J_{2h}, for a given R group, is substantially greater when X = Br than when X = Cl.

In this paper, we report the structure and magnetic properties of a new member of the A_2CuX_4 series, where A is the dication of 3-aminopicoline. In these salts, the perovskite layer severely distorts in order to accommodate this dication. Because of the small length of the dication, significant interlayer coupling is present.

Experimental Procedures

Synthesis. To 0.01 mol of 3-picolylamine and 0.01 mol of anhydrous copper(II) chloride (or copper (II) bromide) were added approximately 25 mL of distilled water and 25 mL of concentrated hydrochloric (or hydrobromic) acid. One week later, crystals of the title compounds were isolated from solution and air dried.

X-ray Crystallographic Studies. The crystal structures of the title compounds were determined. A crystal of size 0.23 × 0.23 × 0.45 mm of the chloride salt was selected for data collection on a Syntex P2_1 spectrometer upgraded to Siemens P4 specifications using graphite-monochromated molybdenum radiation (λ(Kα) = 0.710 73 Å). A crystal of size 0.23 × 0.30 × 0.25 mm of the bromide salt was selected for data collection on a Syntex R3 spectrometer upgraded to Siemens P4 specifications using graphite-monochromated copper radiation (λ(Kα) = 1.541 82 Å). Crystallographic data are reported in Table 1. The unit cell parameters and final orientation matrices for both compounds were obtained from least-squares refinement of 26 machine-centered reflections. During the data collection, the intensities of three standard reflections, monitored every 97 reflections, showed no systematic variations. Data collection and data reduction were performed by utilizing the XSCANS program.[9] Systematic absences suggested the space groups *Pnam* or *Pna*2_1. Intensity statistics indicated the accentric space group, and the structure solution was pursued in the space group *Pna*2_1. This choice was confirmed by the final structure which could not accommodate a mirror plane perpendicular to the *c* axis (vide infra). The intensity data were corrected for Lorentz and polarization effects, and empirical absorption corrections based on Ψ-scan data were applied. The structures were solved via direct methods, followed by difference Fourier synthesis and refined by full-matrix least-square procedures. The data structure refinements were performed with the SHELXTL-PLUS

Table 2. Atomic Coordinates (×10^4) and Equivalent Isotropic Displacement Coefficients (Å × 10^3) for (3-picoliniumylammonium)$CuCl_4$

atom	*x*	*y*	*z*	*U*(eq)[a]
Cu(1)	1206(1)	3213(1)	39	30(1)
Cu(2)	−3761(1)	4791(1)	159(1)	32(1)
Cu(3)	2283(1)	6542(1)	61(1)	33(1)
Cl(9)	1195(4)	6573(1)	1315(2)	37(1)
Cl(10)	1221(4)	6588(1)	−1153(2)	45(1)
Cl(5)	−5926(3)	4143(1)	170(2)	34(1)
Cl(8)	−3505(4)	4694(1)	−1175(2)	41(1)
Cl(7)	−1753(3)	5454(1)	148(2)	39(1)
Cl(11)	3560(3)	7348(1)	93(2)	40(1)
Cl(6)	−3853(4)	4803(1)	1495(2)	53(1)
Cl(1)	−963(3)	3814(1)	266(2)	37(1)
Cl(2)	1159(4)	3391(1)	−1276(2)	45(1)
Cl(3)	3394(3)	2605(1)	−156(2)	42(1)
Cl(4)	1428(4)	3059(1)	1380(2)	43(1)
Cl(12)	3213(3)	5682(1)	97(2)	48(1)
N(1)	−964(14)	8225(4)	6229(6)	45(3)
C(1)	−1644(19)	8359(6)	7000(8)	57(5)
C(2)	−354(16)	8362(5)	7645(6)	37(4)
C(3)	235(16)	8866(5)	7963(7)	48(4)
C(4)	1324(16)	8845(5)	8590(8)	49(4)
C(5)	1837(17)	8395(5)	8915(8)	45(4)
N(2)	1271(13)	7922(4)	8619(6)	46(4)
C(6)	184(15)	7904(4)	7994(7)	41(4)
N(3)	1125(14)	1603(4)	8961(6)	43(3)
C(7)	1708(18)	1844(6)	8206(7)	51(4)
C(8)	360(16)	1752(4)	7549(6)	32(3)
C(9)	−368(15)	2187(5)	7169(7)	40(4)
C(10)	−1419(14)	2108(4)	6566(6)	35(4)
C(11)	−1810(19)	1634(6)	6313(8)	52(5)
N(4)	−1110(13)	1162(4)	6675(6)	52(4)
C(12)	−45(15)	1235(4)	7297(6)	33(3)
N(5)	5958(11)	277(3)	9216(5)	39(3)
C(13)	6781(18)	126(7)	8476(7)	60(5)
C(15)	5576(11)	28(4)	7827(6)	34(3)
C(18)	4941(18)	−478(4)	7667(8)	50(4)
C(17)	3873(18)	−557(5)	7014(9)	62(5)
C(16)	3375(18)	−149(6)	6571(8)	62(5)
N(6)	3978(12)	340(3)	6753(6)	46(3)
C(14)	5018(16)	440(5)	7330(6)	37(3)

[a] Equivalent isotropic *U* defined as one-third of the trace of the orthogonalized $\mathbf{U}_{ij}$ tensor.

(6) Chow, C.; Chang, K.; Willett, R. D. *J. Chem. Phys.* **1973**, *59*, 2629.
(7) (a) Snively, L. O.; Seifert, P. L.; Emerson, K.; Drumheller, J. E. *Phys. Rev. B.* **1979**, *20*, 2101. (b) Snively, L. O.; Tuthill, G.; Drumheller, J. E. *Phys. Rev. B.* **1981**, *24*, 5349. (c) Rubenacker, G. V.; Waplak, S.; Hutton, S. L.; Haines, D. N.; Drumheller, J. E. *J. Appl. Phys.* **1985**, *57*, 3341.
(8) (a) Straatman, P.; Bloch, R.; Jansen, L. *Phys. Rev. B.* **1984**, *29*, 1414. (b) Bloch, R.; Jansen, L. *Phys. Rev. B.* **1982**, *26*, 148.
(9) XSCANS program, version 2.0a, Siemens Analytical X-ray Instruments Inc., Madison, WI, 1992.
(10) Sheldrick, G. M. SHELXTL-PLUS program, Version 4.0, Siemens Analytical X-ray Instruments Inc., Madison, WI, 1990.

Table 3. Atomic Coordinates ($\times 10^4$) and Equivalent Isotropic Displacement Coefficients (Å $\times 10^3$) for (3-picoliniumylammonium)$CuBr_4$

atom	*x*	*y*	*z*	*U*(eq)[a]
Cu(1)	1147(2)	3223(1)	38	26(1)
Cu(2)	−3785(2)	4814(1)	149(2)	28(1)
Cu(3)	2275(3)	6549(1)	52(2)	28(1)
Br(9)	1143(2)	6573(1)	1348(2)	33(1)
Br(10)	1157(2)	6604(1)	−1231(2)	36(1)
Br(5)	−5957(2)	4141(1)	172(2)	29(1)
Br(6)	−3580(2)	4718(1)	−1271(2)	36(1)
Br(7)	−1706(2)	5474(1)	115(2)	32(1)
Br(11)	3635(2)	7352(1)	82(2)	34(1)
Br(8)	−3918(2)	4854(1)	1547(2)	44(1)
Br(1)	−1023(2)	3841(1)	278(2)	32(1)
Br(2)	1066(2)	3401(1)	−1363(2)	39(1)
Br(3)	3326(2)	2600(1)	−184(2)	37(1)
Br(4)	1370(2)	3072(1)	1449(2)	40(1)
Br(12)	3247(2)	5683(1)	52(2)	39(1)
N(1)	−959(18)	8214(6)	6252(9)	52(6)
C(1)	−1575(23)	8373(8)	6960(12)	55(7)
C(2)	−281(19)	8383(5)	7622(8)	26(5)
C(3)	268(22)	8826(6)	7920(10)	41(6)
C(4)	1351(21)	8834(5)	8549(10)	41(6)
C(5)	1857(21)	8387(6)	8879(10)	40(6)
N(2)	1336(19)	7939(6)	8572(10)	54(6)
C(6)	268(22)	7934(6)	7965(10)	45(6)
N(3)	1057(21)	1593(5)	8925(8)	55(6)
C(7)	1598(27)	1812(8)	8178(10)	60(7)
C(8)	287(21)	1756(6)	7535(8)	34(5)
C(9)	−393(19)	2161(5)	7204(9)	34(5)
C(10)	−1431(18)	2101(5)	6600(9)	26(5)
C(11)	−1810(19)	1653(6)	6317(10)	38(6)
N(4)	−1162(20)	1230(7)	6638(9)	59(6)
C(12)	−52(20)	1280(6)	7256(9)	38(5)
N(5)	5925(14)	287(5)	9159(7)	33(4)
C(13)	6753(23)	140(9)	8411(10)	58(8)
C(15)	5558(15)	43(6)	7794(9)	29(5)
C(18)	4935(30)	−452(6)	7638(12)	64(8)
C(17)	3848(23)	−531(7)	6997(14)	57(8)
C(16)	3423(21)	−126(8)	6572(11)	47(7)
N(6)	3958(12)	321(5)	6731(8)	31(4)
C(14)	5031(22)	419(5)	7321(9)	36(5)

[a] Equivalent isotropic *U* defined as one-third of the trace of the orthogonalized $\mathbf{U}_{ij}$ tensor.

crystallographic package.[10] All non-hydrogen atoms were refined with anisotropic displacement parameters to give $R = 5.21\%$ (chloride salt) and $R = 4.47\%$ (bromide salt). Hydrogen atoms in both compounds were included at idealized locations. Tables 2 and 3 give the positional and thermal parameters for the title compounds. Bond distances and angles for the copper halide network are given in Tables 4−6, respectively.

Magnetic Susceptibility Studies. The susceptibility data from 4.4 to 285 K of powder samples of both compounds were taken with a Lake Shore 7225 susceptometer at a frequency of 375 Hz and an ac excitation field of 0.4 Oe. EPR measurements on powdered samples of both compounds were taken with a Bruker EP300 X-band spectrometer at a microwave frequency of 9.3 GHz at room temperature. The average *g* values obtained from these measurements were used to fit the susceptibility data.

Structure Description

The structures consist of severely distorted antiferrodistortive perovskite layers linked by the 3-picoliniumylammonium dications. As will be shown below, the structures show features of both the (3-ammoniopyridinium)CuX_4 structures[5a] and the structure of $[(CH_3)_2CHNH_3]_2CuCl_4$.[11,12] The structures can be visualized as being built up of ribbons cut from the usual layer

Table 4. Copper−Halide Distances (Å) and Angles (deg) in the Primary Coordination Sphere

Distances			
Cu(1)−Cl(1)	2.285(3)	Cu(1)−Br(1)	2.427(3)
Cu(1)−Cl(2)	2.283(3)	Cu(1)−Br(2)	2.448(3)
Cu(1)−Cl(3)	2.300(3)	Cu(1)−Br(3)	2.436(3)
Cu(1)−Cl(4)	2.325(3)	Cu(1)−Br(4)	2.458(3)
Cu(2)−Cl(5)	2.330(2)	Cu(2)−Br(5)	2.492(3)
Cu(2)−Cl(8)	2.294(4)	Cu(2)−Br(6)	2.454(4)
Cu(2)−Cl(7)	2.271(2)	Cu(2)−Br(7)	2.416(3)
Cu(2)−Cl(6)	2.278(4)	Cu(2)−Br(8)	2.402(4)
Cu(3)−Cl(9)	2.298(4)	Cu(3)−Br(9)	2.407(4)
Cu(3)−Cl(10)	2.230(4)	Cu(3)−Br(10)	2.386(4)
Cu(3)−Cl(11)	2.245(2)	Cu(3)−Br(11)	2.371(2)
Cu(3)−Cl(12)	2.264(2)	Cu(3)−Br(12)	2.397(2)
Angles			
Cl(1)−Cu(1)−Cl(2)	91.5(1)	Br(1)−Cu(1)−Br(2)	91.2(1)
Cl(1)−Cu(1)−Cl(3)	178.5(1)	Br(1)−Cu(1)−Br(3)	179.2(1)
Cl(2)−Cu(1)−Cl(3)	90.0(1)	Br(2)−Cu(1)−Br(3)	89.6(1)
Cl(1)−Cu(1)−Cl(4)	89.8(1)	Br(1)−Cu(1)−Br(4)	89.6(1)
Cl(2)−Cu(1)−Cl(4)	176.3(1)	Br(2)−Cu(1)−Br(4)	176.8(1)
Cl(3)−Cu(1)−Cl(4)	88.7(1)	Br(3)−Cu(1)−Br(4)	89.6(1)
Cl(5)−Cu(2)−Cl(8)	89.8(1)	Br(5)−Cu(2)−Br(6)	89.5(1)
Cl(5)−Cu(2)−Cl(7)	177.2(1)	Br(5)−Cu(2)−Br(7)	179.1(1)
Cl(8)−Cu(2)−Cl(7)	90.6(1)	Br(6)−Cu(2)−Br(7)	90.1(1)
Cl(5)−Cu(2)−Cl(6)	88.7(1)	Br(5)−Cu(2)−Br(8)	89.0(1)
Cl(8)−Cu(2)−Cl(6)	173.7(1)	Br(6)−Cu(2)−Br(8)	176.4(1)
Cl(7)−Cu(2)−Cl(6)	91.2(1)	Br(7)−Cu(2)−Br(8)	91.4(1)
Cl(9)−Cu(3)−Cl(10)	136.5(1)	Br(9)−Cu(3)−Br(10)	134.8(1)
Cl(9)−Cu(3)−Cl(11)	96.2(1)	Br(9)−Cu(3)−Br(11)	97.8(1)
Cl(10)−Cu(3)−Cl(11)	98.0(1)	Br(10)−Cu(3)−Br(11)	98.3(1)
Cl(9)−Cu(3)−Cl(12)	97.1(1)	Br(9)−Cu(3)−Br(12)	98.7(1)
Cl(10)−Cu(3)−Cl(12)	101.0(1)	Br(10)−Cu(3)−Br(12)	100.5(1)
Cl(11)−Cu(3)−Cl(12)	135.2(1)	Br(11)−Cu(3)−Br(12)	132.9(1)

Table 5. Semicoordinate Copper−Halide Distances (Å) and Angles (deg)[a]

Distances			
Cu(1)−Cl(5d)	3.220	Cu(1)−Br(5d)	3.370
Cu(1c)−Cl(3)	3.005	Cu(1c)−Br(3)	3.168
Cu(2d)−Cl(1o)	3.270	Cu(2d)−Br(1o)	3.399
Cu(2d)−Cl(12)	3.233	Cu(2d)−Br(12)	3.319
Cu(3d)−Cl(7d)	4.144	Cu(3d)−Br(7d)	4.289
Cu(3e)−Cl(11)	4.000	Cu(3e)−Br(11)	4.124
Angles			
Cu(1)−Cl(5d)−Cu(2d)	175.0	Cu(1)−Br(5d)−Cu(2d)	175.1
Cu(1)−Cl(3)−Cu(1c)	165.3	Cu(1)−Br(3)−Cu(1c)	164.1
Cu(2d)−Cl(1o)−Cu(1d)	165.4	Cu(2d)−Br(1o)−Cu(1d)	165.2
Cu(2d)−Cl(12)−Cu(3)	152.1	Cu(2d)−Br(12)−Cu(3)	152.4
Cu(2d)−Cl(7d)−Cu(3d)	174.0	Cu(2d)−Br(7d)−Cu(3d)	175.4
Cu(3)−Cl(11)−Cu(3e)	159.9	Cu(3)−Br(11)−Cu(3e)	161.9

[a] c denotes atom coordinates transformed by $0.5 + x$, $0.5 - y$, z; d denotes atom coordinates transformed by $1 + x$, y, z; e denotes atom coordinates transformed by $0.5 + x$, $^3/_2 - y$, z; o denotes atom coordinates transformed by $1 + x$, y, z.

Table 6. Interlayer Halide−Halide Distances (Å) and Angles (deg)[a]

Distances			
Cl(4a)−Cl(2d)	4.760	Br(4a)−Br(2d)	4.556
Cl(6a)−Cl(8b)	4.641	Br(6a)−Br(8b)	4.404
Cl(9a)−Cl(2c)	4.494	Br(9a)−Br(2c)	4.317
Angles			
Cu(1a)−Cl(4a)−Cl(2d)	143.7	Cu(1a)−Br(4a)−Br(2d)	142.8
Cu(2a)−Cl(6a)−Cl(8b)	150.7	Cu(2a)−Br(6a)Br−(8b)	151.6
Cu(3a)−Cl(9a)−Cl(2c)	177.4	Cu(3a)−Br(9a)−Br(2c)	177.8

[a] a denotes atom coordinates transformed by $x - 1$, y, z; b denotes atom coordinates transformed by $-x - 1$, $-y$, $0.5 + z$; c denotes atom coordinates transformed by $-x - 1$, $-y$, $0.5 + z$; d denotes atom coordinates transformed by $-x - 1$, $1 - y$, $z + 0.5$.

(11) (a) Anderson, D. N.; Willett, R. D. *Inorg. Chim. Acta* **1974**, *8*, 167. (b) Swank, D. D.; Landee, C. P.; Willett, R. D. *J. Magn. Mater.* **1980**, *15*−*18*, 319. (c) Bloomquist, D. R.; Willett, R. D. *J. Phys. Chem. Solids* **1981**, *42*, 455.

(12) Willett, R. D. *Acta Crystallogr.* **1988**, *C44*, 2071.

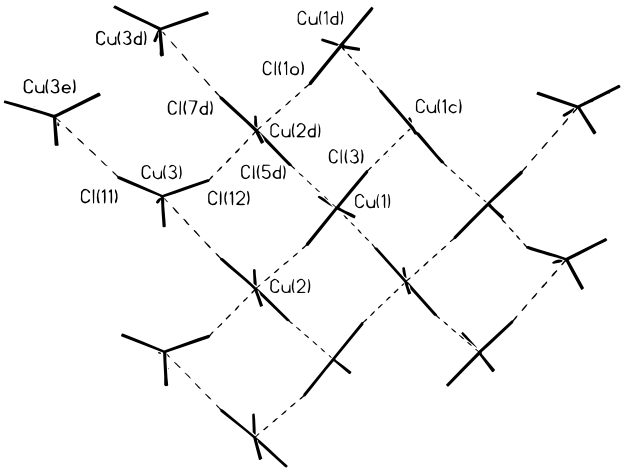

Figure 1. Illustration of the CuX_4 "ribbons". (The *a* axis is vertical, and the *b* axis is horizontal.)

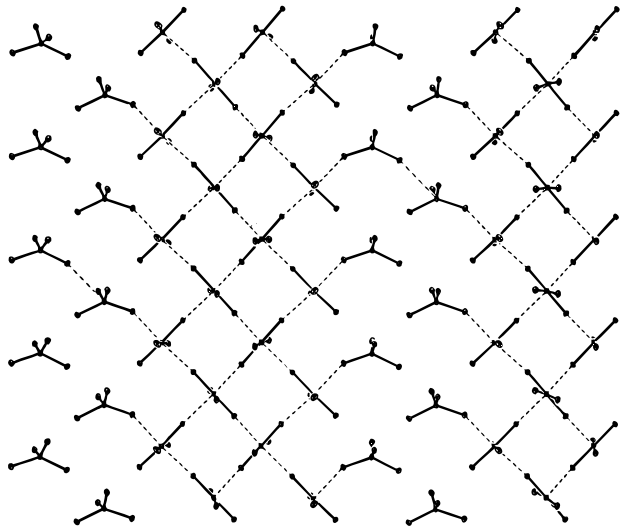

Figure 2. Illustration of the CuX_4 "sheets". (The *a* axis is vertical, and the *b* axis is horizontal.)

perovskite structures. These ribbons, illustrated in Figure 1 for the Cl salt, are six copper atoms wide. The ribbons, which lie athwart the *a* glide planes perpendicular to *b*, run parallel to the *a* axis. The central four copper atoms (labeled Cu(1) and Cu(2)) retain their usual elongated octahedral coordination with four short Cu−X bonds (2.296 Å average for X = Cl and 2.442 Å average for X = Br). However the copper atoms on the edges of the ribbons (labeled Cu(3)) have a significant tetrahedral distortion imposed upon their coordination geometry and are probably better described as CuX_4^{2-} anions with flattened tetrahedral geometry. The "*trans*" X−Cu−X angles are approximately 136° for X = Cl and 134° for X = Br. Extremely long Cu···X interactions exist between the Cu(3) and X(7) atoms (4.144 and 4.289 Å for Cl and Br, respectively) which retain the antiferrodistortive nature of the atomic arrangements within the ribbons. A similar ribbon structure exists in the above mentioned $[(CH_3)_2CHNH_3]_2CuCl_4$ structure.[11] However in that case the ribbons are only three copper atoms wide, so only one of the copper atoms retains its distorted octahedral geometry.

The ribbons arrange themselves into layers lying parallel to the *ab* plane as illustrated in Figure 2. In this manner, the CuX_4^{2-} anions on the edges of the ribbons lie adjacent to each other. Again the general antiferrodistortive nature of the layers is retained by formation of additional extremely long Cu···X contacts between the Cu(3) and X(11) (Figure 1) atoms (4.000 Å for X = Cl and 4.124 Å for X = Br). This is in contrast to the ribbon arrangement in the $[(CH_3)_2CHNH_3]_2CuCl_4$ structure,[11] where adjacent ribbons are rotated approximately 90° about the ribbon axis.

Three-dimensional stability is given to the structure by hydrogen bonding between the 3-picoliniumylammonium dications and the halide ions in the layers, with the dications bridging between adjacent layers. This is illustrated in Figure 3. Two modes of hydrogen bonding are present. The $-CH_2-NH_3^+$ moieties are involved in a traditional type of interaction in which the N atoms sit in the center of a box formed by four X atoms which protrude out of the layers, and the three H atoms are all involved in hydrogen bonds to X atoms to both terminal and bridging X atoms.[13] It is not nearly as favorable for the pyridinium rings to form hydrogen bonds to bridging X atoms. Nevertheless, by forcing an exceptional elongation of the semicoordinate Cu···X bonds, it is able to do so. The only previously known examples are in the (3-ammoniopyridinium)-CuX_4 structures.[5a]

Examination of Figure 3 also demonstrates the nonexistence of a mirror plane perpendicular to the *c* axis, as would be required in the centrosymmetric space group option. The low symmetry of the cation restricts the location of the potential

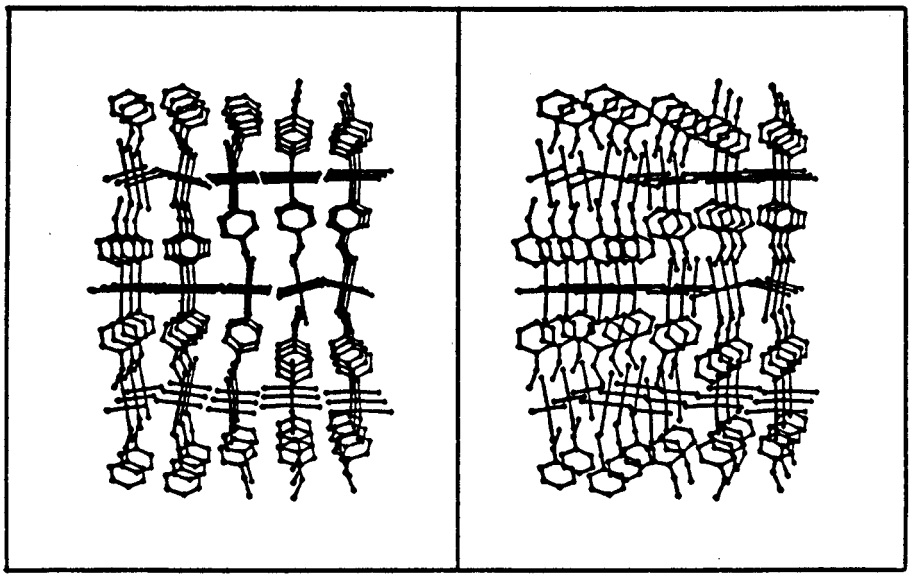

Figure 3. Stereo illustration of the 3-dimensional network. (The *b* axis is vertical, and the *c* axis is horizontal.)

mirror planes to the arrangements coincident with the planes defined by the layers of the Cu(II) ions. However, the repeat pattern for one of the three unique pyridinium cations chains (center column in Figure 3) is such that the potential for mirror symmetry is destroyed.

The hydrogen bonding configuration for the dications forces the layers into a so-called "eclipsed" arrangement[12] in which the terminal halide ions in adjacent layers lie directly on top of each other. This leads to relatively short X···X distances between layers as is shown in Figure 4. Significantly, these interlayer distances shorten when Cl is replace by Br (4.629 Å average for Cl versus 4.425 Å average for Br). As a result, the volume available for the dications remains essentially constant between the two salts, due to the increase in the distances within the layers.

EPR Analysis

Powder EPR spectra were obtained for both salts. The spectrum for the bromide salt consisted of a single broad line centered at $g = 2.14$ with peak-to-peak line width of approximately 500 Oe at room temperature. The line width for the chloride salt was considerably narrower, and a rhombic spectrum was observed with principle g values of $g_1 = 2.066$, $g_2 = 2.135$, and $g_3 = 2.230$. Assuming strong exchange coupling in the compound, these can be identified with the g values along the three crystallographic axes.

The local geometries of the Cu(II) ions are such that one expects local g values of $g_\perp \approx 2.04-2.05$ and $g_{||} \approx 2.27-2.30$ for Cu(1) and Cu(2),[5a] while Cu(3) should have $g_\perp \approx 2.06-2.08$ and $g_{||} \approx 2.35-2.40$.[14] The orientations of the coordination polyhedra (see Figure 1) are such that $g_{||}$ always lie approximately in the (010) plane, with $g_{||}$ for Cu(1) and Cu(2) oriented ±45° from *a*, respectively. Thus we anticipate the following approximate crystal g values:

$$g_a = {}^1/_3[\{\cos^2 45 g_\perp(1) + \sin^2 45 g_{||}(1)\} + \{\cos^2(-45) g_\perp(2) + \sin^2 45 g_{||}(2)\} + g_{||}(3)] \approx {}^1/_3(2.16 + 2.16 + 2.40) \approx 2.24$$

$$g_b = {}^1/_3[g_\perp(1) + g_\perp(2) + g_\perp(3)] \approx {}^1/_3[2.04 + 2.04 + 2.06] = 2.05$$

$$g_c = {}^1/_3[\{\sin^2 45 g_\perp(1) + \cos^2 45 g_{||}(1)\} + \{\sin^2(-45) g_\perp(2) + \cos^2(-45) g_{||}(2)\} + g_\perp(3)] \approx {}^1/_3(2.16 + 2.16 + 2.06) \cong 2.13$$

Thus the observed rhombic **g** tensor for the chloride salt is in qualitative agreement with the expectation based on the crystal geometry.

Magnetic Behavior and Exchange Pathways

Several different types of exchange pathways can be identified in the structure. Three general categories exist: (1) the interactions within the ribbons of the copper atoms with distorted octahedral coordination via their semicoordinate bonds; (2) the interactions of copper atoms with tetrahedral geometries with neighbors within or between ribbons; (3) two-halide Cu−X···X−Cu interactions between layers.

The first type of exchange pathway, labeled J_1, involves Cu(1) and Cu(2), both of which assume the typical "4 + 2" distorted octahedral geometries found in the copper(II) halide layer perovskite structures. The exchange pathways through the semicoordinate linkages can be assumed to be ferromagnetic. It has been shown that the strength of this interaction decreases monotonically with the length of the semicoordinate Cu···X distances.[5] There are four of this type of pathway (see Figure 1): Cu(1)−X(3)···Cu(1c), Cu(1d)−X(1o)···Cu(2d), Cu(2d)−X(5d)···Cu(1), and Cu(3)−X(12)···Cu(2d). From the correlations reported,[5] we can predict $J_1/k \approx 11$ and 20 K for X = Cl and Br, respectively, on the basis of the average Cu···X distances of 3.182 and 3.314 Å, respectively.

The J_2 pathways involve interactions of the tetrahedral copper atoms with halide ions on adjacent CuX_4^{2-} anions. Two such pathways exist: Cu(2d)−X(7d)···Cu(3d) at the edges of the ribbons and Cu(3)−X(11)···Cu(3e) between adjacent ribbons. In each case, the bridging halide ion approaches Cu(3) across one of its tetrahedral faces. Previously, this group reported the structure and magnetic behavior of $[(CH_3)_2CHNH_3]CuCl_4$,[11] which illustrates a similar X···M bridging. In this structure, the bridging halide's approach to the metal ion across one of the tetrahedral faces leads to short (3.62 and 3.85 Å average) X···X contacts in the two independant chains. Analysis of the magnetic behavior found in the narrower ribbon structure of $[(CH_3)_2CHNH_3]CuCl_4$ suggests that these short X··X contacts lead to predominantely antiferromagnetic coupling.[11b] In the (3-picoliniumylammonium)CuX_4 structure, however, the two halide contacts that arise from these bridiging ligands are significantly longer (4.254 and 4.101 Å for the Cu(2d)−Cl(7d)···Cu(3d) and Cu(3)−Cl(11)···Cu(3e) pathways, respec-

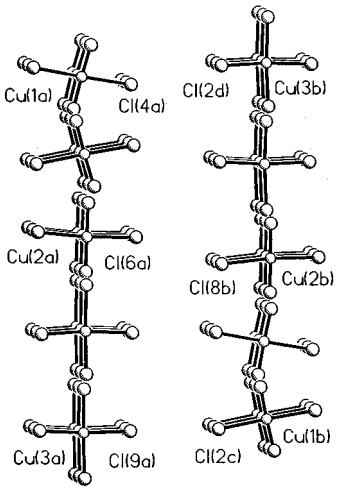

Figure 4. Illustration of the interlayer Cu−X···X−Cu exchange pathways. (The *b* axis is vertical, and the *c* axis is horizontal.)

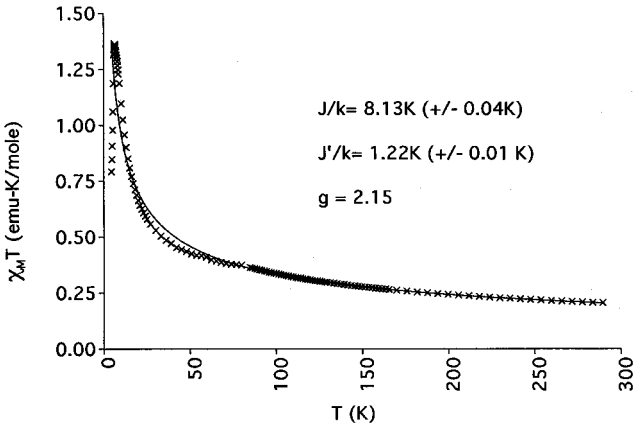

Figure 5. Plot of χT_M versus T for $(C_6N_2H_{10})CuCl_4$. (Experimental data = ×, and best fit = −.)

(13) Chapuis, G.; Arend, H.; Kind, R. *Phys. Status Solidi A* **1975**, *31*, 449.
(14) Gaura, R. M.; Stein, P.; Willett, R. D.; West, D. X. *Inorg. Chim. Acta* **1982**, *60*, 213 and references therein.

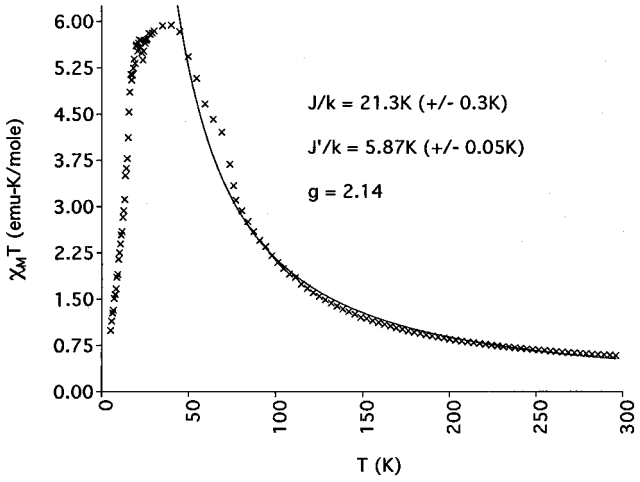

Figure 6. Plot of χT_M versus T for $(C_6N_2H_{10})CuBr_4$. (Experimental data = ×, and best fit = —.)

tively) than in the $[(CH_3)_2CHNH_3]CuCl_4$ structure. This increased X···X contact distance, coupled with a comparision of the Cu−X···X bridging angles between the two structures, suggests that Cu−X···Cu interactions are predominant in the J_2 pathway in the 3-picolyamine compound and that these intereactions are ferromagnetic in nature.

The J_3 pathways, which are illustrated in Figure 4, involve halide−halide contacts between adjacent layers. These interactions, which are invariably antiferromagnetic, have been studied extensively by Drumheller et al.[7] They have been shown to decrease monotonically with increasing X···X distance, both theoretically[8] and experimentally.[12] With average Cl···Cl distances of 4.632 Å and Br···Br distances of 4.426 Å, we expect to find $J_3/k \approx 1.65$ K for X = Cl and $J_3/k \approx 14.12$ K for X = Br.

The magnetic susceptibility data of $(C_6N_2H_{10})CuCl_4$ and $(C_6N_2H_{10})CuBr_4$ (Figures 5 and 6) show evidence of two types of magnetic interaction: a dominant FM exchange at high temperature which causes χT to increase with decreasing temperatures and a weaker AFM exchange that becomes important at lower temperatures which tends to align the resultant moments antiparallel. The Cl and Br salts undergo antiferromagnetic ordering at $T_c = 5.7$ and 18.9 K, respectively. The susceptibility data above T_c for both compounds were fit to a high-temperature series expansion Heisenberg model[14] based on the Hamiltonian $H = -2\sum J_{ij}S_i \bullet S_j$ that incorporates a two dimensional intralayer FM exchange coupling and AFM exchange coupling between layers. The mean in-plane exchange constants derived from the fitting, which are associated with the aforementioned J_1 and J_2 pathways, are $J/k = 8.1$K and $J/k = 21.3$ K for the Cl and Br salts. The interlayer exchange constants, associated with the J_3 pathways, are $J'/k = -1.2$ K for the Cl salt and $J'/k = -5.8$ K for the Br salt. The exchange constants for both materials are in reasonable agreement with those predicted by Willett and co-workers[5] as outlined in the previous paragraphs.

Conclusions

The title compounds are characterized as new members of the copper halide antiferrodistortive layer perovskite family. Due to the unique structural characteristics of the 3-picolylamine dication, significant hydrogen bonding can occur between the cations and the halide atoms. This hydrogen bond stabilization of the structure gives rise to the extreme distortion of the classic layer perovskite framework which has been seen previously only in the (3-ammoniopyridinium)CuX_4 structures.

Acknowledgment. The authors acknowledge Prof. J. E. Drumheller and Kala Subberaman at Montana State University for the use of the Lakeshore susceptometer.

Supporting Information Available: Tables S1−S12 gives crystal data and details of the structure determination, anisotropic thermal parameters, bond angles and distances, and hydrogen atom coordinates and a figure showing a unit cell (17 pages). Ordering information is given on any current masthead page.

IC960849+